



Preparation of thermosensitive magnetic liposome encapsulated recombinant tissue plasminogen activator for targeted thrombolysis



Hao-Lung Hsu^a, Jyh-Ping Chen^{a,b,c,d,*}

^a Department of Chemical and Materials Engineering, Chang Gung University, Kwei-San, Taoyuan 33302, Taiwan, ROC

^b Department of Plastic and Reconstructive Surgery and Craniofacial Research Center, Chang Gung Memorial Hospital, Kwei-San, Taoyuan 33305, Taiwan, ROC

^c Graduate Institute of Health Industry and Technology, Research Center for Industry of Human Ecology, Chang Gung University of Science and Technology, Kwei-San, Taoyuan 33302, Taiwan, ROC

^d Department of Materials Engineering, Ming Chi University of Technology, Tai-Shan, New Taipei City 24301, Taiwan, ROC

ARTICLE INFO

Keywords:

Magnetic nanoparticles
Magnetic liposomes
Tissue plasminogen activator
Thermosensitive
Drug delivery

ABSTRACT

Recombinant tissue plasminogen activator (rtPA) was encapsulated in thermosensitive magnetic liposome (TML) prepared from 1,2-dipalmitoyl-*sn*-glycero-3-phosphocholine, distearoylphosphatidyl ethanolamine-*N*-poly(ethylene glycol) 2000, cholesterol and Fe₃O₄ magnetic nanoparticles by solvent evaporation/sonication and freeze-thaw cycles method. Response surface methodology was proved to be a powerful tool to predict the drug encapsulation efficiency and temperature-sensitive drug release. Validation experiments verified the accuracy of the model that provides a simple and effective method for fabricating TML with controllable encapsulation efficiency and predictable temperature-sensitive drug release behavior. The prepared samples were characterized for physico-chemical properties by dynamic light scattering, transmission electron microscopy, X-ray diffraction and differential scanning calorimetry. Temperature-sensitive release of rtPA could be confirmed from *in vitro* thrombolysis experiments. A thrombolytic drug delivery system using TML could be proposed for magnetic targeted delivery of rtPA to the site of thrombus followed by temperature-triggered controlled drug release in an alternating magnetic field.

1. Introduction

Venous thromboembolism is a silent yet potentially fatal disease that affects millions annually. The best way to improve patient survival and to decrease rate and extent of morbidity is prompt and early treatment of thromboembolism using an effective thrombolytic therapy. Plasminogen activators are used to trigger the dissolution of thrombi (thrombolysis) by catalyzing the conversion of plasminogen to the protease plasmin, which then digests fibrin and lyses the clot. Streptokinase [1,2], urokinase [3,4] and recombinant tissue plasminogen activator (rtPA) [5,6] are plasminogen activators used clinically in the treatment of established thrombus. Since rtPA binds preferentially to plasminogen entrapped in fibrin, it is more effective, safer and useful for thrombolytic therapy [7].

However, plasminogen activators are immunogenic and have short half-lives because of their foreign nature, which requires administration of large doses of rtPA to obtain therapeutic effects and inevitably leads to a significant incidence of hemorrhagic side effects as a consequence [8]. By encapsulating plasminogen activators within novel

carrier systems, an increased half-life and decreased immunogenicity might be achieved. Furthermore, targeted delivery of the thrombolytic agent under magnetic guidance for target thrombolysis followed by controlled drug release may reduce the risks of hemorrhage and toxicity associated with systemic administration, thus offering a promising, minimally invasive approach that could decrease the total administered dose of the drug necessary for the treatment and hence its complications [9].

Liposomal vehicle for the delivery of drugs is actively being investigated and has been proposed for thrombus-specific delivery of plasminogen activators to extend the half-life and to reduce hemorrhagic side effects [10,11]. Recent studies showed that thermosensitive liposomes can significantly increase the efficiency of antitumor drug release with hyperthermia, using triggered drug release near the gel-to-liquid crystalline phase transition temperature of the lipids [12]. Upon heating, liquid–solid boundaries start to form in the lipid bilayer and the drug could be released from the internal aqueous compartment or the lipid bilayer [13]. The PEG-derived carriers can reduce the uptake of liposomes by the reticuloendothelial system and are expected to

* Corresponding author at: Department of Chemical and Materials Engineering, Chang Gung University, Kwei-San, Taoyuan 33302, Taiwan, ROC.
E-mail address: jpchen@mail.cgu.edu.tw (J.-P. Chen).

<http://dx.doi.org/10.1016/j.jmmm.2016.10.122>

Received 26 June 2016; Received in revised form 19 October 2016; Accepted 23 October 2016

Available online 26 October 2016

0304-8853/ © 2016 Elsevier B.V. All rights reserved.

prolong the half-lives of plasminogen activators in blood [14]. On the other hand, magnetic liposomes (magnetic nanoparticles encapsulated within liposomes) are widely used to encapsulate drugs and genes [15,16], which could provide an effective magnetic targeted delivery system.

In this work, we propose a more efficient thrombolytic drug delivery system using PEGylated thermosensitive magnetic liposomes (TMLs) for magnetic targeted delivery of rtPA to the site of thrombus followed by temperature-triggered controlled drug release in an alternative magnetic field. rtPA-loaded TMLs were prepared from 1,2-dipalmitoyl-*sn*-glycero-3-phosphocholine (DPPC), distearoylphosphatidyl ethanolamine-*N*-poly(ethylene glycol) 2000 (DSPE-PEG₂₀₀₀) and cholesterol by solvent evaporation/sonication and freeze-thaw cycles method. The object was to optimize the formulation of TML-rtPA using response surface methodology (RSM) [17,18]. The experimental parameters or variables considered were the molar percentage of DPPC/lipid, DSPE-PEG/lipid and cholesterol/lipid, and the molar ratio of lipid/magnetic nanoparticle and the results of the experiments were the drug encapsulation efficiency (EE) and the release percentages of rtPA at 37 °C and 43 °C. The effects of the variables were investigated within the context of RSM that incorporates design of experiments and non-linear regression. This approach enables experimental investigation of individual factors and the interactions of factors simultaneously as opposed to one-factor-at-a-time approach. Models of EE and release percentage of rtPA at 37 °C and 43 °C were constructed, which could allow the evaluation of the significance of the parameters and provide the prediction capability for EE and temperature-modulated drug release.

2. Materials and method

2.1. Materials

Fe(II) chloride tetrahydrate (99%) and Fe(III) chloride hexahydrate (97%) were purchased from Acros. DPPC was acquired from Avanti Polar Lipids, Inc. (USA). DSPE-PEG₂₀₀₀ was obtained from NOF Co. (Japan). Cholesterol and Triton X-100 were purchased from Sigma-Aldrich Co. (USA). Recombinant tissue plasminogen activator (rtPA) was purchased from Boehringer Ingelheim (Germany). All chemicals were of reagent grade and used without further purification.

2.2. Synthesis of iron oxide (Fe₃O₄) magnetic nanoparticles (MNPs)

The chemical co-precipitation method of Fe²⁺ and Fe³⁺ ions (molar ratio of 1:2) by addition of NH₄OH was used for synthesis of Fe₃O₄ magnetic nanoparticles (MNPs) [19]. 0.875g of FeCl₂·4H₂O and 2.375g of FeCl₃·6H₂O were mixed in 40 ml of double-distilled water (DDI water) and stirred at 400 rpm in a three-neck flask. The temperature was increased to 60 °C in refluxing condition under N₂ atmosphere and kept for 10 min. Five milliliters of 25% NH₄OH was added and pH of the solution was maintained at 10 with vigorous stirring for 60 min. The black-colored colloidal MNPs were recovered by magnetic separation and dialyzed against DDI water (3.5 kDa MWCO) to remove excess of NH₄OH.

2.3. Preparation of thermosensitive magnetic liposomes (TML) and rtPA-encapsulated TML (TML-rtPA)

The TML-rtPA was prepared by the solvent evaporation/freezing-thaw method [20,21]. Lipid mixtures of DPPC, DSPE-PEG₂₀₀₀ and cholesterol in various molar composition were dissolved in 1 ml chloroform/methanol solution (2:1, v/v) to form a 10 mM solution. The organic solvent was removed using a rotary evaporator (EYELA N-1200AVF, Japan) at 100 psi and 45 °C with a water bath for 10 min. The solvent was then completely removed in a vacuum oven overnight to from a thin phospholipid film on the wall of the round-bottom flask.

The resulting dry film was hydrated with 1 ml of DDI water containing various concentrations of MNP and 0.1 mg/ml rtPA and rotated for 60 min. The solution was removed and sonicated at 200 W for 5 min using a Q500 sonicator (Qsonica, Newton, CT, USA) at 4 °C in a water bath. The sample was flash frozen in liquid nitrogen and thawed completely at room temperature. This freeze-thaw cycle was repeated five times for maximum encapsulation of rtPA. Finally, un-encapsulated rtPA was removed by ultracentrifugation for 30 min at 30,000 rpm and 20 °C.

2.4. Determination of encapsulation efficiency of rtPA in TML-rtPA

The rtPA encapsulation efficiency in TML-rtPA was determined using a Protein Assay Kit from Bio-Rad (USA). The TML-rtPA was disrupted with 1% Triton X-100 solution and diluted with 0.01 M phosphate buffer (pH 7.4) before measurements. The encapsulation efficiency of rtPA was calculated from the following equation,

$$\text{Encapsulation efficiency (\%)} = \frac{W_E}{W_{\text{total}}} \times 100 \quad (1)$$

where W_{total} is the amount of rtPA added and W_E is the amount of rtPA encapsulated.

2.5. In vitro release of rtPA

The *in vitro* release behavior of rtPA from TML-rtPA was determined as follows. TML-rtPA (5 mg) was prepared in 1 ml of phosphate buffered saline (PBS, pH 7.4) at 37 °C or 43 °C and shaken at 120 rpm. At predetermined time, the solution was centrifuged at 30,000 rpm for 30 min and 0.5 ml of the supernatant was removed. The solution was supplemented with 0.5 ml of fresh PBS, re-suspended and incubated at the same condition as before. The amount of rtPA in the supernatant was determined by the Protein Assay Kit as described before. The percentage of rtPA released was calculated using the following equation,

$$\text{Release of rtPA (\%)} = \frac{W_{\text{release}}}{W_E} \times 100 \quad (2)$$

where W_E is the amount of rtPA encapsulated and W_{release} is the amount of rtPA released.

2.6. Experimental design

The RSM as a generic means for optimization was applied to optimize the formulation of TML-rtPA [22]. The optimization was designed based on a five-level, four-factor central composite rotatable design (CCRD) with a total of 31 experimental runs that combined 16 factorial points, 8 axial points and 7 replicates at the center points. Based on the preliminary experiments and our previous studies, the effect of four formulation independent variables, DPPC/lipid molar percentage (X_1), DSPE-PEG₂₀₀₀/lipid molar percentage (X_2), cholesterol/lipid molar percentage (X_3) and lipid/MNP molar ratio (X_4) were identified as key factors responsible for EE and rtPA release percentage after 60 min at 37 °C and 43 °C. In view of the feasibility of liposome preparation and drug loading ratio for clinical doses, the ranges of the four factors were determined as follows: X_1 , 60/92; X_2 , 1/5; X_3 , 5/33; X_4 , 100/1000 (Table 1). Each experimental run was performed in duplicate except at the central point (25–31 runs) of the design. According to the mathematical model, the response surface could be related to the selected variables by a second-order polynomial model as in the following equation,

$$Y_i = \alpha_0 + \sum_i \alpha_i X_i + \sum_i \alpha_{ii} X_i^2 + \sum_{i \neq j} \alpha_{ij} X_i X_j \quad (3)$$

where Y_i represents the predicted responses, X_i and X_j are the coded values of independent variables, α_0 is the intercept coefficient, α_i are

Table 1
Independent variable and their levels used in central composite rotatable design.

Factors	Codes	Variable levels				
		2	-1	0	-1	-2
DPPC/lipid percentage	X ₁	92	84	76	68	60
DSPE-PEG2000/lipid percentage	X ₂	5	4	3	2	1
Cholesterol/lipid percentage	X ₃	33	26	19	12	5
Lipid/MNP ratio	X ₄	10,000	7525	5050	2575	100

the linear coefficients, α_{ii} are the squared coefficients and α_{ij} are the interaction coefficients.

The quality of fit of the model was evaluated by the analysis of variances (ANOVA) and the coefficients of determination (R^2) that was the fraction of the data explained by the model. All calculations were coded in Statistica software (Stat-Ease Inc., USA).

2.7. Characterization of TML and TML-rtPA

The particles sizes and zeta potentials of vesicles were determined by dynamic light scattering (DLS) using a Zetasizer Nano ZS (Malvern Instruments Ltd., Worcestershire, UK). The DLS analysis was performed at a scattering angle of 173° and 25 °C in the auto-measuring mode. Particles dispersions were dilute with DDI water for size measurements and 10 mM phosphate buffer (pH 7.4) for zeta potential measurements. The morphology and particle size of Fe₃O₄ MNPs were measured by transmission electron microscopy (TEM, JEOL JEM-2000 EX II) at an acceleration voltage of 100 kV. The liposomes were dispersed with DDI water and drop-cast onto a 300 mesh carbon-coated copper grid and dried at 25 °C before loading into the microscope. The morphology and particle size of TML and TML-rtPA were determined by cryo-TEM. The liposomes were prepared at 10 mM lipids. The samples were drop-cast onto a 300 mesh carbon-coated copper grid and rapidly frozen by plunge-freezing in liquid ethane cooled by liquid nitrogen using a Cryoplunger™ 3 (Gatan Inc.). The cryo-fixed specimens were mounted into a Gatan cryoholder (Model 914, Gatan Inc.) for direct observation at -170 °C at 120 kV using a JEOL JEM-1400 TEM.

For X-ray diffraction (XRD) analysis of the crystallographic characteristic of vesicles, a D₂ Phaser X-ray powder diffractometer (Bruker, WI, USA) was used by scanning in the 2θ range of 20–70° with Cu K_α radiation. The step size was 0.05° and the measuring time was 2 s per step. The phase was compared with the JCPDS database. The crystallite size was determined from the strongest (311) reflection using the Scherrer equation [23],

$$D = \frac{K \times \lambda}{\beta \times \cos \theta} \quad (4)$$

where D is the average size of the crystalline domains, K is a dimensionless shape factor, normally taken as 0.9, λ is the wavelength of X-ray in nanometer (nm), β is the peak width of the diffraction peak profile at half maximum height intensity (FWHM), θ is the Bragg angle. For differential scanning calorimetry (DSC) analysis, 10 μl of hydrated liposomes (DPPC, TML and TML-rtPA) were placed in a 20 μl DSC aluminum pan and analyzed with a Q20 DSC (TA Instruments). The scan rate was 5 °C/min from 25 to 50 °C.

2.8. In vitro thrombolysis

Citrated whole blood from Sprague-Dawley (SD) rats (BioLasco Co., Taiwan) was obtained by cardiac puncture under anesthesia with isoflurane. Rat blood (900 μl) and thrombin solution (100 μl, 50 U/ml) were mixed in a polyethylene tube with an internal diameter of 1 mm. The tube was incubated vertically at room temperature for 10 min and cut into cylindrical shapes with 5 mm length. The formed

Table 2
Central composite design arrangement and response.

Design point	Coded independent variable levels				Response value		
	X ₁	X ₂	X ₃	X ₄	E.E. (%)	Release, 37 °C (%)	Release, 43 °C (%)
1	-1	-1	-1	-1	70.2	19.8	19.2
2	1	-1	-1	-1	62.8	15.5	22.1
3	-1	1	-1	-1	60.1	18.0	23.2
4	1	1	-1	-1	72.9	11.8	14.2
5	-1	-1	1	-1	62.8	25.1	27.3
6	1	-1	1	-1	46.2	36.9	44.6
7	-1	1	1	-1	67.1	20.1	22.2
8	1	1	1	-1	61.5	22.3	28.5
9	-1	-1	-1	1	62.2	20.6	27.0
10	1	-1	-1	1	64.2	17.2	22.4
11	-1	1	-1	1	67.7	14.1	17.8
12	1	1	-1	1	72.4	10.2	18.2
13	-1	-1	1	1	66.8	22.1	33.4
14	1	-1	1	1	58.2	27.5	35.5
15	-1	1	1	1	66.9	22.0	31.2
16	1	1	1	1	61.4	23.3	27.9
17	-2	0	0	0	62.9	23.8	30.2
18	2	0	0	0	63.7	19.5	25.8
19	0	-2	0	0	53.6	19.8	29.1
20	0	2	0	0	56.6	19.2	26.1
21	0	0	-2	0	65.9	14.1	19.7
22	0	0	2	0	61.4	27.1	37.5
23	0	0	0	-2	66.0	20.5	30.1
24	0	0	0	2	67.7	25.2	27.8
25	0	0	0	0	61.1	22.8	49.9
26	0	0	0	0	60.7	21.7	27.6
27	0	0	0	0	63.6	25.0	29.1
28	0	0	0	0	63.6	22.6	28.0
29	0	0	0	0	60.3	19.9	28.7
30	0	0	0	0	59.6	27.5	37.2
31	0	0	0	0	63.8	23.1	27.6

X₁=DPPC/lipid molar percentage; X₂=DSPE-PEG2000/lipid molar percentage; X₃=cholesterol/lipid molar percentage; X₄=lipid/MNP molar ratio.

blood clots were extruded from the tube and washed with PBS. One blood clot (1×5 mm) was used for thrombolysis in a 4 ml vial. The vial contained free rtPA or TML-rtPA (2 μg rtPA) in 1 ml PBS were incubated statically at 37 °C or 43 °C for 30 min. The supernatant was removed from the vial and the absorbance at 415 nm (OD₄₁₅) was measured to calculate the amount of hemachrome (hemoglobin) as an indication of the extent of thrombolysis by rtPA [11].

3. Results and discussion

3.1. Model development of EE and drug release at different temperatures

A CCRD with four variables was employed to design the experiments. The design of CCRD was according to statistical theory with 2⁴ factorial consists of 31 experiments, including 16 factorial points (cubic point, -1 and +1) and 8 axial points (star point, -2 and +2) as well as seven replicates at the center point. Seven replications (treatments 25–31) at the center of the design were used to estimate the pure error sum of squares. As shown in Table 2, the results at each point gives the experimental data of the response value based on experimental design, i.e. EE and release percentage after 60 min at 37 °C and 43 °C. The runs were randomized for statistical reasons. The choice of 37 °C and 43 °C represents the normal body temperature and the temperature subject to hyperthermia with TML in an alternating magnetic field.

The Pareto chart shown in Fig. 1 graphically illustrates the effects of variables on EE and the release percentage. The length of each bar was proportional to the absolute value of its associated regression coefficient or estimated effect. The order in which the bars were displayed

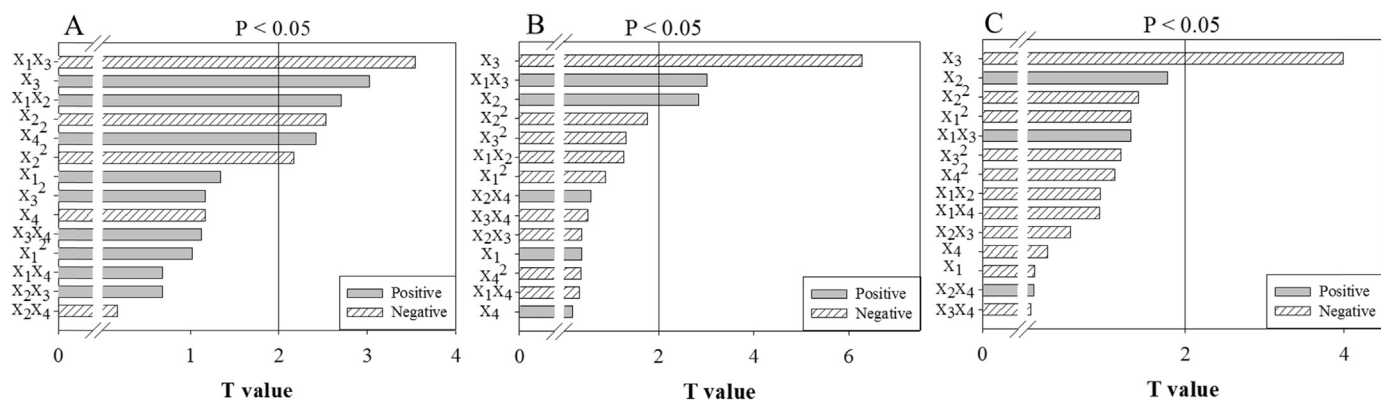


Fig. 1. Pareto chart of standardized effect for the model of encapsulation efficiency (A), and release percentage at 37 °C (B) and 43 °C (C). The line indicates the confidence level of 95%, and factors with standardized effect values to the right of this line are statistically significant.

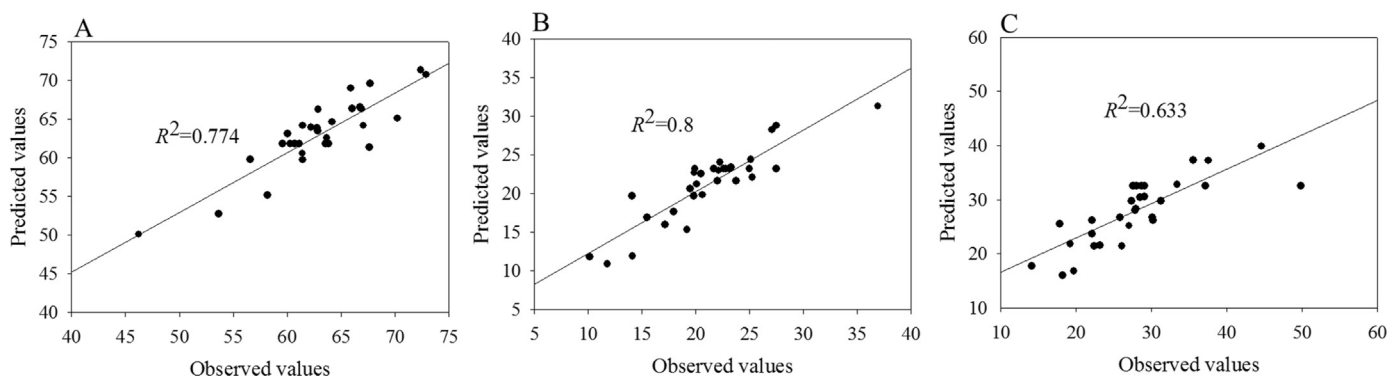


Fig. 2. Predicted values over observed values of encapsulation efficiency (A), and release percentage at 37 °C (B) and 43 °C (C).

Table 3 Results of model validation experiments.

Factors	Codes	Variable	Predicted values			Experimental values		
			EE (%)	Release, 37 °C (%)	Release, 43 °C (%)	EE (%)	Release, 37 °C (%)	Release, 43 °C (%)
DPPC	X ₁	80	65.1	22.2	30.6	64.7 ± 1.6	21.0 ± 1.8	31.4 ± 2.5
DSPE-PEG2000	X ₂	5						
Cholesterol	X ₃	5						
Lipid/MNP	X ₄	100						

Table 4 Physicochemical properties of thermosensitive magnetic liposome.

Sample	Size from DLS (nm)	Zeta potential (mV)	MNP diameter (nm)	
			TEM	XRD
MNP	181 ± 17	-15.5 ± 0.4	10.7 ± 1.0	13.5
TML	303 ± 13	-8.4 ± 0.4	10.2 ± 2.1	12.2
TML-rtPA	443 ± 26	-5.7 ± 0.3	9.8 ± 1.9	13.1

corresponded to the order of the size of the effect. The chart included a vertical line that corresponded to the 95% limit indicating statistical significance. A factor was, therefore, significant if its corresponding bar crossed this vertical line [17]. From Fig. 1A, two linear coefficients (X₂, X₃), two cross-product coefficients (X₁X₂, X₁X₃) and two quadratic coefficients (X₂², X₄²) were found to be significant (p < 0.05). Fig. 1B showed two linear coefficients (X₂, X₃) and one cross-product coefficient (X₁X₃) to be significant (p < 0.05), while Fig. 1C had only one linear coefficient (X₃) to be significant (p < 0.05).

The data were fitted to a response surface model to effectively evaluate the true relationship between the response values and the factors following the statistical method. According to the estimation of

data, a second-order regression model was obtained by using coded values,

$$Y_1 = 121.11 - 1.427X_1 - 16.696X_2 + 3.294X_3 - 0.006X_4 + 0.289X_1X_2 - 0.054X_1X_3 + 0.084X_2X_3 + 0.01X_1^2 - 1.389X_2^2 + 0.015X_3^2 \quad (5)$$

$$Y_2 = -10.45 + 0.894X_1 + 17.628X_2 - 2.997X_3 + 0.001X_4 - 0.126X_1X_2 + 0.043X_1X_3 - 0.044X_2X_3 - 0.008X_1^2 - 1.051X_2^2 - 0.016X_3^2 \quad (6)$$

$$Y_3 = -150.05 + 3.836X_1 + 27.96X_2 - 2.035X_3 + 0.007X_4 - 0.181X_1X_2 + 0.036X_1X_3 - 0.122X_2X_3 - 0.024X_1^2 - 1.647X_2^2 - 0.028X_3^2 \quad (7)$$

where Y₁ is the EE response value, Y₂ is the drug release at 37 °C and Y₃ is the drug release at 43 °C. X_i is the coded value of each factor.

The R² values are 0.774, 0.8 and 0.633 for EE and drug release at 37 °C and 43 °C, respectively. These values indicate the percentage of variability of all response that is explained by the model and the models are able to be applied in the subsequent prediction stages. From Fig. 1A, it could be concluded that the linear effect of X₂ and X₃, the cross-product effect of X₁X₂, X₁X₃, and the quadric effect of X₂², X₄² were the primary determining factors of response Y₁. From Fig. 1B, it could be concluded that the linear effect of X₂, X₃, and the cross-

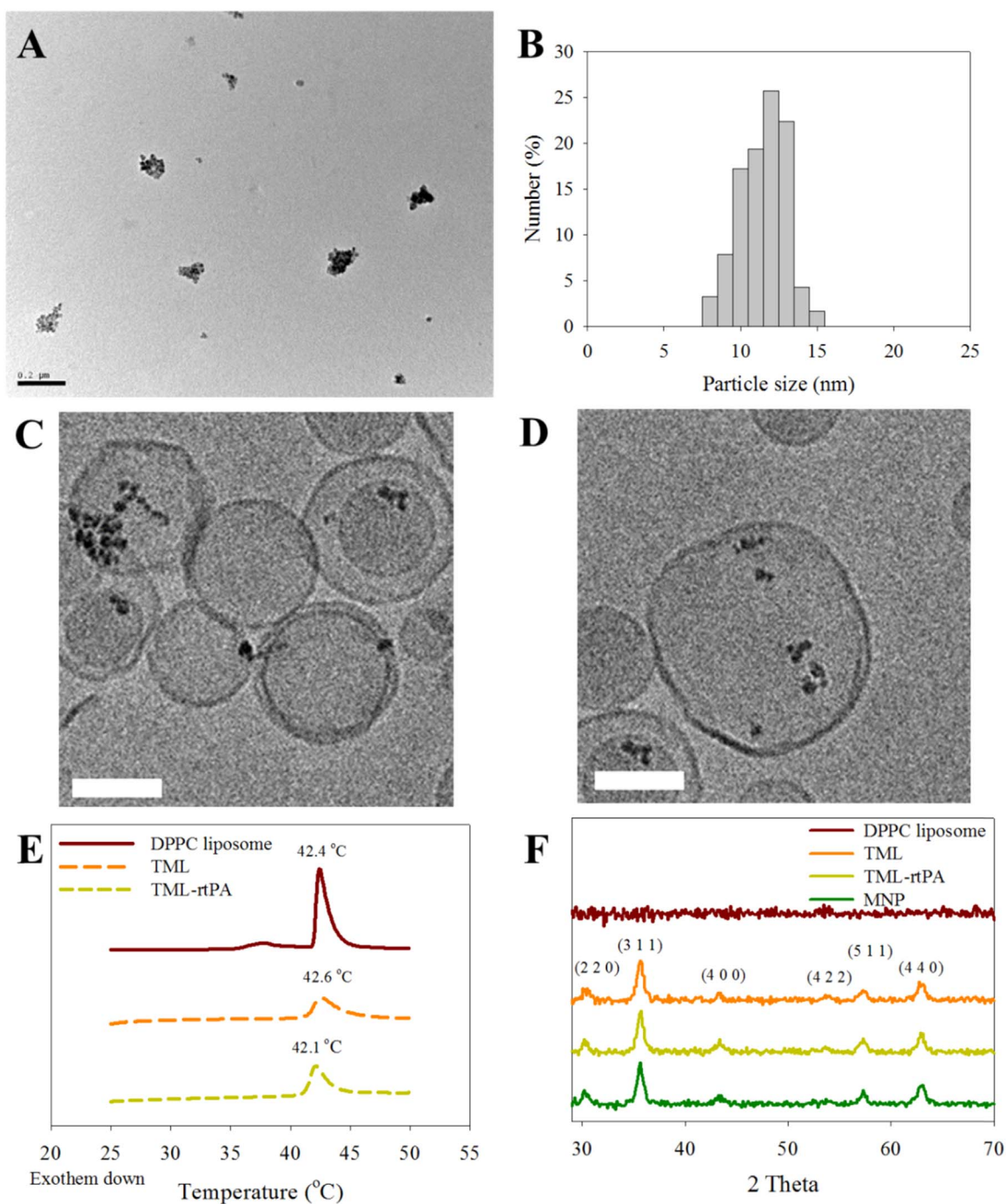


Fig. 3. Transmission electron microscope (TEM) image (A) (bar=200 nm) and particle size distribution (B) of Fe₃O₄ magnetic nanoparticle (MNP). Cryo-TEM images of thermosensitive magnetic liposome (TML) (C) and thermosensitive magnetic liposome encapsulating rtPA (TML-rtPA) (D) (bar=200 nm). (E) DSC analysis of DPPC liposome, TML and TML-rtPA. (F) XRD analysis of DPPC liposome, TML and TML-rtPA and Fe₃O₄ MNP.

product effect of X_1X_3 were the primary determining factors of the response Y_2 . From Fig. 1C, it could be concluded that the linear effect of X_3 was the primary determining factor of response Y_3 .

To evaluate the optimization technique, the observed values of EE and release percentages in Table 2 are compared with the predicted values in Fig. 2. As can be seen, the predicted values of the response from the model accorded well with the observed experimental values. The experimental findings were in close agreement with the prediction model in view of the correlation between theoretical predicted values and experimental values. Although the model coefficients obtained are empirical, which cannot be associated with physical or chemical significance; they are very useful to predict the results of untested

operation conditions [20].

To confirm the correlation and significance of Eqs. (5)–(7), the adequacy of the model was examined using additional independent experiments that were not employed in the model generation. The predicted EE and release percentages at 37 °C and 43 °C are 65.1%, 30.6% and 22.2%, respectively, with the combination of factors in Table 3. As shown in Table 3, the experimental and predicted values show good agreement with the average absolute relative deviation being 1.4%, 0.8% and 1.2%. The average EE and release percentages at 37 °C and 43 °C are $64.7 \pm 1.6\%$, $31.4 \pm 2.5\%$ and $21.0 \pm 1.8\%$ (mean \pm SD, $n=6$), respectively. The mean of the experimental value is reasonably close to the predicted one, which confirmed the validity and

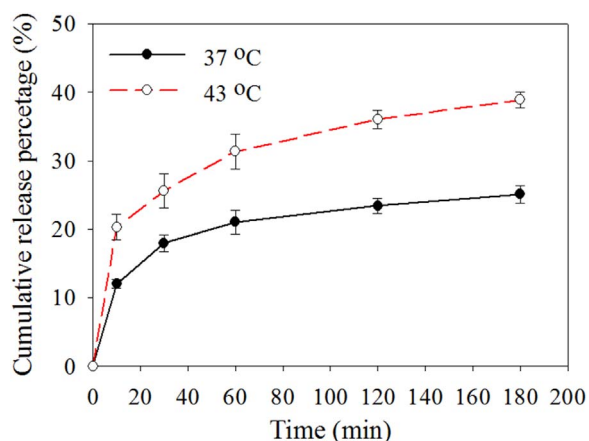


Fig. 4. *In vitro* cumulative release of rtPA from TML-rtPA in PBS (pH 7.4) at 37 °C and 43 °C.

adequacy of the predictive model.

3.2. Characterization of TML-rtPA

The chemical co-precipitation of ferric and ferrous salts in an alkaline medium was used for the preparation of Fe_3O_4 MNP. As shown in Table 4, the mean hydrodynamic diameters of MNP and TML obtained by DLS were 181 and 303 nm, respectively, which was significantly different from that of TML-rtPA (443 nm). Encapsulation of protein molecules (rtPA) in TML therefore lead to an increase of liposome diameter [24]. From the electrophoretic mobility measurements, the zeta potential of MNP increased from -15.5 mV to -8.4 mV due to encapsulated in positively charged lipids, which further increased to -5.7 mV after encapsulation of positively charged protein rtPA (Table 4).

From Fig. 3A, the TEM micrograph of aggregated MNP showed a size around 130 nm to be slightly lower than that from DLS measurement. Nonetheless, discrete MNP could still be observed from the TEM image with the particle size distribution shown in Fig. 3B. The average size of MNP could be calculated to be 10.7 nm (Table 4), indicating superparamagnetic nanoparticles. The internal structures of TML and TML-rtPA were characterized by cryo-TEM. Fig. 3C and D indicate uniform spherical morphology of TML and TML-rtPA with diameters being 300 and 400 nm, respectively. The larger size of TML-rtPA is consistent with DLS measurements. The average size of the discrete MNP in TML and TML-rtPA was estimated to be around 10 nm (Table 4). The Fourier transform infrared spectroscopy (FTIR) and

superconducting quantum interference device (SQUID) analysis shown in Supplementary material indicate the incorporation of DPPC/ Fe_3O_4 MNP in TML and the superparamagnetic property of TML-rtPA.

The DSC data (Fig. 3E) show a thermal curve with a sharp transition peak at 42.1 °C for TML-rtPA, which could be comparable to 42.6 °C and 42.4 °C for TML and liposomes prepared from the thermosensitive lipid DPPC [25]. This confirms that encapsulation of MNP and rtPA did not affect the phase transition temperature of DPPC and the thermos-sensitivity of the liposome. It should be noted that a pre-transition is observed at 37.7 °C for DPPC liposomes, which can be assigned to the transition from a crystalline gel phase to a rippled gel phase, in addition to the sharp phase peak displayed in liquid disordered or liquid-crystalline phase. Upon addition of cholesterol to the bilayer in TML, the pre-transition is no longer detected due to the interactions between the cholesterol polar groups and DPPC head groups.

The XRD patterns of MNP, TML and TML-rtPA are illustrated in Fig. 3F. All samples have six characteristic peaks at $2\theta=30.11^\circ$, 35.41° , 43.11° , 53.21° , 56.91° and 62.51° , which can be indexed to the (220), (311), (400), (422), (511), and (440) planes of a cubic cell. The crystalline structure of the particle can be confirmed to correspond to that of a magnetite structure (JCPDS card number 19-0629) and reveals that all resultant nanoparticles were pure Fe_3O_4 with a spinel structure of the magnetite. It is also evident that the lipid-coating process and rtPA-encapsulation did not result in a phase change of Fe_3O_4 MNP. The average crystal grain sizes are from 12.2 to 13.5 nm (Table 4), calculated from the Scherrer equation with XRD line broadening assuming crystals are spherical. The diffraction peak corresponding to (311) was used since it is well resolved and shows no interferences.

3.3. In vitro temperature-sensitive release of rtPA and thrombolysis

The cumulative release curves of rtPA from TML-rtPA in PBS at 37 and 43 °C are shown in Fig. 4. An initial burst release is observed at 10 min and is modulated by temperature as expected for TML. A higher temperature triggers a higher drug release rate and release percentages were 12% and 21% at 37 and 43 °C, respectively. A sustained release behavior follows and cumulative release percentages at 180 min reached 25% and 39% at 37 and 43 °C, respectively. This suggested that release of rtPA from TML-rtPA could be controlled by MNP-based hyperthermia under an applied alternating magnetic field after magnetic guidance of TML-rtPA to the thrombus site for targeted thrombolysis *in vivo*.

To further illustrate this controlled release for thrombolysis of

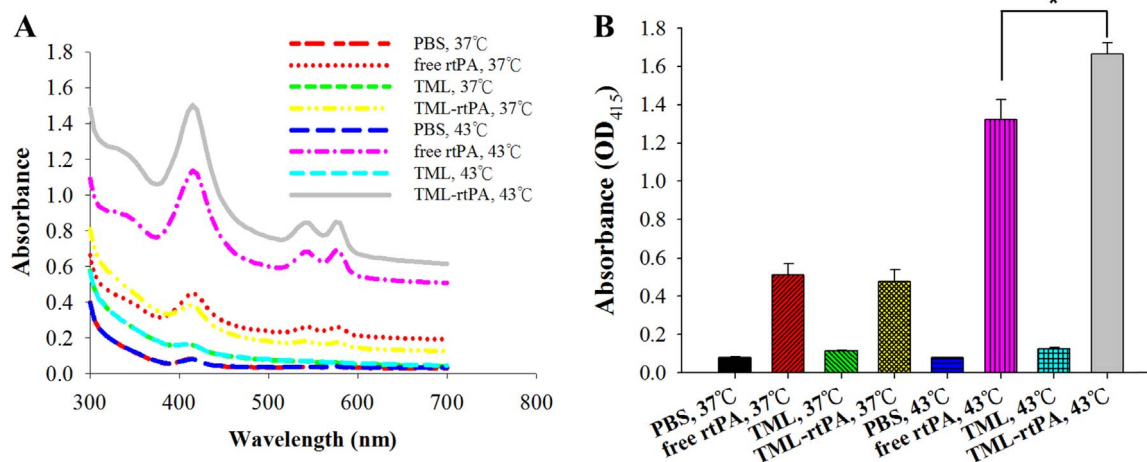


Fig. 5. *In vitro* thrombolysis at 37 °C and 43 °C subject to different treatments. (A) After a blood clot was treated for 30 min, the supernatant was subject to full spectrum absorbance scans. (B) The OD_{415} due to released hemoglobin from the blood clot after different treatments was compared for the efficiency of thrombolysis. 2 $\mu\text{g}/\text{ml}$ rtPA was used. *: $p < 0.05$.

blood clot. The blood clot lysis was investigated for PBS, free rtPA, TML or TML-rtPA at 37 °C and 43 °C (Fig. 5). After 30 min of reaction, the supernatant was subject to full spectrum absorbance scans (Fig. 5A). The highest peak at 415 nm due to released hemoglobin from the blood clot (OD₄₁₅) was compared in Fig. 5B for the efficiency of thrombolysis. Control experiments in PBS and with TML indicate minimum OD₄₁₅ values from background thrombolysis. Free rtPA and TML-rtPA show no significant difference in OD₄₁₅ values at 37 °C, which are 0.51 ± 0.06 and 0.48 ± 0.06 . Although the *in vitro* release drug experiment in Fig. 4 does not indicate full release of rtPA protein after 60 min, the full retention of thrombolytic activity may be due to the intimate mixing of TML-rtPA with the clot, which led to disruption of liposome and protein release within the matrix [26]. In contrast, OD₄₁₅ values at 43 °C are 1.32 ± 0.11 and 1.66 ± 0.06 for free rtPA and TML-rtPA, respectively. That the thrombolytic activity of TML-rtPA at 43 °C is higher than that of TML-rtPA at 37 °C was due to the combined effects of enhanced drug release and enzyme activity at a higher temperature. Nonetheless, the significant difference in clot lysis activity between free rtPA and TML-rtPA indicates temperature-sensitive drug release at the thrombus site will be a feasible strategy for controlled release of rtPA in an alternating magnetic field *in vivo*.

4. Conclusions

RSM was proved to be a powerful tool for predicting the encapsulation efficiency and temperature-sensitive release of rtPA from TML-rtPA. A second-order model was obtained to describe the relationship between the obtained response and the operating parameters. Validation experiments verified the accuracy of the model, which provided a simple and effective method for fabricating TML-rtPA with maximum drug loading and controllable drug release. Successful preparation of TML-rtPA with encapsulated rtPA was demonstrated from analysis of its physico-chemical properties. The effect of temperature on drug release was confirmed from *in vitro* drug release and thrombolysis experiments. TML-rtPA developed in this study will be useful as a magnetic targeted nanodrug with temperature-responsive drug release to improve clinical thrombolytic therapy.

Acknowledgements

Financial supports from the Ministry of Science and Technology (MOST), Taiwan, ROC (NSC102-2221-E-182-046) and Chang Gung Memorial Hospital (BMRP249, CMRPD250023) are acknowledged.

Appendix A. Supplementary material

Supplementary data associated with this article can be found in the online version at [doi:10.1016/j.jmmm.2016.10.122](https://doi.org/10.1016/j.jmmm.2016.10.122).

References

- [1] G. Damaschun, H. Damaschun, K. Gast, D. Gerlach, R. Misselwitz, H. Welfle, D. Zirwer, Streptokinase is a flexible multi-domain protein, *Eur. Biophys. J.* 20 (1992) 355–361.
- [2] B. Holt, A.S. Gupta, Streptokinase loading in liposomes for vascular targeted nanomedicine applications: encapsulation efficiency and effects of processing, *J. Biomater. Appl.* 26 (2012) 509–527.
- [3] H. Jin, H. Tan, L. Zhao, W. Sun, L. Zhu, Y. Sun, H. Hao, H. Xing, L. Liu, X. Qu, Y. Huang, Z. Yang, Ultrasound-triggered thrombolysis using urokinase-loaded nanogels, *Int. J. Pharm.* 434 (2012) 384–390.
- [4] J.N. Marsh, G. Hu, M.J. Scott, H. Zhang, M.J. Goette, P.J. Gaffney, S.D. Caruthers, S.A. Wickline, D. Abendschein, G.M. Lanza, A fibrin-specific thrombolytic nanomedicine approach to acute ischemic stroke, *Nanomedicine* 6 (2011) 605–615.
- [5] S. Absar, S. Choi, F. Ahsan, E. Cobos, V.C. Yang, Y.M. Kwon, Preparation and characterization of anionic oligopeptide-modified tissue plasminogen activator for triggered delivery: an approach for localized thrombolysis, *Thromb. Res.* 131 (2013) e91–e99.
- [6] S. Absar, Y.M. Kwon, F. Ahsan, Bio-responsive delivery of tissue plasminogen activator for localized thrombolysis, *J. Control. Release* 177 (2014) 42–50.
- [7] S. Absar, K. Nahar, Y.M. Kwon, F. Ahsan, Thrombus-targeted nanocarrier attenuates bleeding complications associated with conventional thrombolytic therapy, *Pharm. Res.* 30 (2013) 1663–1676.
- [8] A. Tadayon, R. Jamshidi, A. Esmaeili, Delivery of tissue plasminogen activator and streptokinase magnetic nanoparticles to target vascular diseases, *Int. J. Pharm.* 495 (2015) 428–438.
- [9] S.T. Laing, M.R. Moody, H. Kim, B. Smulevitz, S.L. Huang, C.K. Holland, D.D. McPherson, M.E. Klegerman, Thrombolytic efficacy of tissue plasminogen activator-loaded echogenic liposomes in a rabbit thrombus model, *Thromb. Res.* 130 (2012) 629–635.
- [10] I.A. Tiebosch, B.J. Crielaard, M.J. Bouts, R. Zwartbol, A. Salas-Perdomo, T. Lammers, A.M. Planas, G. Storm, R.M. Dijkhuizen, Combined treatment with recombinant tissue plasminogen activator and dexamethasone phosphate-containing liposomes improves neurological outcome and restricts lesion progression after embolic stroke in rats, *J. Neurochem.* 123 (Suppl 2) (2012) S65–S74.
- [11] E. Voros, M. Cho, M. Ramirez, A.L. Palange, E. De Rosa, J. Key, Z. Garami, A.B. Lumsden, P. Decuzzi, TPA immobilization on iron oxide nanocubes and localized magnetic hyperthermia accelerate blood clot lysis, *Adv. Funct. Mater.* 25 (2015) 1709–1718.
- [12] M. de Smet, S. Langereis, S. van den Bosch, H. Grull, Temperature-sensitive liposomes for doxorubicin delivery under MRI guidance, *J. Control. Release* 143 (2010) 120–127.
- [13] L. Li, T.L. ten Hagen, D. Schipper, T.M. Wijnberg, G.C. van Rhoon, A.M. Eggermont, L.H. Lindner, G.A. Koning, Triggered content release from optimized stealth thermosensitive liposomes using mild hyperthermia, *J. Control. Release* 143 (2010) 274–279.
- [14] J.Y. Kim, J.K. Kim, J.S. Park, Y. Byun, C.K. Kim, The use of PEGylated liposomes to prolong circulation lifetimes of tissue plasminogen activator, *Biomaterials* 30 (2009) 5751–5756.
- [15] P. Pradhan, J. Giri, F. Rieken, C. Koch, O. Mykhaulyk, M. Doblinger, R. Banerjee, D. Bahadur, C. Plank, Targeted temperature sensitive magnetic liposomes for thermo-chemotherapy, *J. Control. Release* 142 (2010) 108–121.
- [16] A. Bakandritsos, A.G. Fatouros, D.G. Fatouros, Magnetoliposomes and their potential in the intelligent drug-delivery field, *Ther. Deliv.* 3 (2012) 1469–1482.
- [17] K.S.B. Cavalcante, M.N.C. Penha, K.K.M. Mendonça, H.C. Louzeiro, A.C.S. Vasconcelos, A.P. Maciel, A.G. de Souza, F.C. Silva, Optimization of transesterification of castor oil with ethanol using a central composite rotatable design (CCRD), *Fuel* 89 (2010) 1172–1176.
- [18] N.K. Rastogi, K.R. Rashmi, Optimisation of enzymatic liquefaction of mango pulp by response surface methodology, *Eur. Food Res. Technol.* 209 (1999) 57–62.
- [19] P. Berger, N.B. Adelman, K.J. Beckman, D.J. Campbell, A.B. Ellis, G.C. Lisensky, Preparation and properties of an aqueous ferrofluid, *J. Chem. Educ.* 76 (1999) 943.
- [20] P. Pradhan, J. Giri, R. Banerjee, J. Bellare, D. Bahadur, Preparation and characterization of manganese ferrite-based magnetic liposomes for hyperthermia treatment of cancer, *J. Magn. Mater.* 311 (2007) 208–215.
- [21] J. Heeremans, H. Gerritsen, S. Meusen, F. Mijneer, R. Gangaram Panday, R. Prevost, C. Kluff, D. Crommelin, The preparation of tissue-type plasminogen activator (t-PA) containing liposomes: entrapment efficiency and ultracentrifugation damage, *J. Drug Target.* 3 (1995) 301–310.
- [22] Y. Xiong, D. Guo, L. Wang, X. Zheng, Y. Zhang, J. Chen, Development of nobililide A loaded liposomal formulation using response surface methodology, *Int. J. Pharm.* 371 (2009) 197–203.
- [23] J.P. Chen, C.H. Liu, H.L. Hsu, T. Wu, Y.J. Lu, Y.H. Ma, Magnetically controlled release of recombinant tissue plasminogen activator from chitosan nanocomposites for targeted thrombolysis, *J. Mater. Chem. B* 4 (2016) 2578–2590.
- [24] M. Koneracká, P. Kopčanský, P. Sosa, J. Bageřová, M. Timko, Interliposomal transfer of crystal violet dye from DPPC liposomes to magnetoliposomes, *J. Magn. Mater.* 293 (2005) 271–276.
- [25] K.J. Fritzsche, J. Kim, G.P. Holland, Probing lipid–cholesterol interactions in DOPC/eSM/Chol and DOPC/DPPC/Chol model lipid rafts with DSC and ¹³C solid-state NMR, *Biochim. Biophys. Acta* 1828 (2013) 1889–1898.
- [26] R. Sabate, R. Barnadas-Rodriguez, J. Callejas-Fernandez, R. Hidalgo-Alvarez, J. Estelrich, Preparation and characterization of extruded magnetoliposomes, *Int. J. Pharm.* 347 (2008) 156–162.